

Co-Design Optimization for Data Center Cooling System via Digital Twin

Shrenik Jadhav

Department of Computer and Information
Science,
University of Michigan-Dearborn,
4901 Evergreen Rd,
Dearborn, MI, USA

Zheng Liu¹

Department of Industrial and Manufacturing
Systems Engineering,
University of Michigan-Dearborn,
4901 Evergreen Rd,
Dearborn, MI, USA
email: zhengtli@umich.edu

Liquid-cooled exascale supercomputers dissipate heat through cooling plants organized as multiple parallel subloops, but how to allocate coolant distribution units (CDUs) across subloops and how to distribute flow among them has not been systematically addressed for facilities at this scale. This paper presents a three-layer optimization framework that jointly determines the integer partition of CDUs across subloops, the continuous flow fraction allocation, and the per-timestep co-design optimization of total flow rate and supply temperature subject to per-subloop thermal safety constraints. The Modelica simulation model is built based on the data of Frontier exascale supercomputer at Oak Ridge National Laboratory. By developing a reduced-order surrogate model, all 611 feasible partitions of 25 CDUs are evaluated across the full year operational dataset of 49,353 timesteps. Three progressively richer operational strategies are compared, ranging from flow control optimization to full three-layer co-design optimization with dynamically adjusted flow fractions. The globally optimal design is a two-subloop plant achieving 35.48% annual cooling energy savings, only 0.18% above the current three-subloop Frontier design at 35.30%. Flow fraction optimization is shown to compensate for any feasible CDU-to-subloop assignment, reducing the design sensitivity by 93% and providing a low-cost software-only pathway to near-optimal performance on the existing Frontier hardware. The framework is transferable to other liquid-cooled high-performance computing plants.

Keywords: Data center, thermal management, co-design optimization, digital twin

1 Introduction

Data center electricity consumption has emerged as one of the most rapidly growing loads on the global power system. World-wide data center demand reached 415 TWh in 2024, approximately 1.5% of total electricity use, and is projected to exceed 945 TWh by 2030 [1]. In the United States, data centers consumed 176 TWh in 2023, about 4.4% of national electricity, with projections ranging from 325 to 580 TWh by 2028 [2]. Cooling infrastructure accounts for 30 to 40% of total facility electricity consumption [3, 4], making it the single largest controllable load in most data centers. Despite a decade of advances in efficient server hardware and air-side economization, the global average Power Usage Effectiveness has remained between 1.55 and 1.59 since 2020 [5], indicating that incremental improvements to existing cooling systems are approaching diminishing returns and that more systematic optimization approaches are needed.

High-performance computing (HPC) facilities experience this challenge at an amplified scale. Exascale supercomputers such as Frontier at Oak Ridge National Laboratory operate at power levels of 8 to 30 MW, employ 100% direct liquid cooling with variable-speed pumps, and exhibit rapid thermal transients driven by workload dynamics [6, 7]. These systems differ structurally from enterprise data centers in three important ways. First, liquid cooling loops respond to load changes on time scales of minutes rather than the seconds typical of forced-air cooling, introducing tight coupling between thermal inertia and actuator rate limits. Second, equipment thermal constraints such as the 45 °C coolant return temperature limit on direct-to-chip cold plates are operationally binding during high-load periods, leaving less margin for aggressive setpoint optimization. Third, the cooling plant architecture at facility scale is organized into multiple parallel subloops,

each with independent pumps and heat exchangers, which creates a combinatorial design space that does not arise in smaller installations.

Despite the scale of energy involved, systematic cooling plant optimization for HPC facilities remains underdeveloped. Existing work on the Frontier system has focused on operational data collection and dataset release [6], system-wide power management [7], thermal stability during load transients [8], waste heat recovery integration [9], and data-driven diagnosis of cooling inefficiency [10]. These studies establish the physical and data foundation for optimization but do not prescribe control or design actions. In our recent work [10], a three-stage machine learning framework was applied to the Frontier 2023 operational dataset to identify cooling energy waste, quantify approximately 85 MWh of annual inefficiency, and demonstrate that up to 96% of the identified excess could be recovered through guardrail-constrained counterfactual setpoint adjustments. That work established the existence and magnitude of cooling energy waste at Frontier but did not construct a physics-based plant model and did not address the plant design question of how the 25 CDUs should be allocated across the parallel subloops.

A complementary line of work addresses cooling plant optimization through physics-based digital twins. The Modelica language and its Buildings Library [11] have become the dominant open-source platform for equation-based modeling of HVAC and cooling systems, and Modelica models have been developed for air-cooled data centers [12, 13], district cooling systems [14], chiller plants with water-side economization [15], and comparative co-design of cooling control strategies [16]. For HPC specifically, the Exascale Digital Twin (ExaDigiT) project at Oak Ridge National Laboratory developed a digital twin of liquid-cooled supercomputers using the TRANSFORM component library in Modelica [17–19]. However, the ExaDigiT effort prioritized verification and validation over systematic optimization, and the question of how to use a validated

¹Corresponding Author.

Version 1.18, May 18, 2026

digital twin as the basis for design-space exploration was left to subsequent work.

Our own recent contribution in this area [20] constructed a Modelica-based digital twin of the Frontier hot-temperature water (HTW) cooling system, validated it against one full calendar year of 10-minute operational data following ASHRAE Guideline 14 [21], and used the validated twin to evaluate three progressively constrained control strategies: a flow-only optimization achieving 20.4% total cooling energy savings, an unconstrained joint optimization of flow rate and supply temperature reaching 30.1%, and a ramp-constrained joint optimization retaining 27.8% (corresponding to a recovery ratio of 92.4% relative to the unconstrained optimum). That work demonstrated that a validated digital twin can serve as an optimization testbed for HPC cooling control, and it quantified the gap between theoretical and deployable control strategies. However, it treated the cooling plant topology as fixed, accepting the existing Frontier design of three active parallel subloops with 14, 6, and 5 CDUs each, while not considering the plant design for co-design optimization.

This research focuses on the co-design optimization for data center. We established a validated digital twin of the Frontier cooling system, and provided the operational control strategies, to optimize the plant configuration for lowering annual cooling energy. The plant design space contains three coupled classes of decisions. The first is the number of parallel subloops K , which determines how the total thermal load is distributed across independent hydraulic branches. The second is the allocation of the 25 CDUs across the K subloops, which is an integer partition problem with 611 feasible configurations for K between 2 and 6. The third is the flow fraction allocation f_k across the subloops, which can be fixed at design time through hydraulic balancing valves or optimized dynamically through independent per-subloop flow control. These three classes of decisions interact through the per-subloop thermal constraint and the shared pump and cooling tower energy cost, producing a mixed-integer nonlinear optimization problem whose structure and solution have not been previously analyzed for an exascale HPC cooling plant.

A related body of work addresses plant-level optimization in chiller plants and district cooling systems, where decisions about equipment sizing, sequencing, and flow distribution have been studied using mixed-integer programming [22, 23], metaheuristic search [24], and surrogate-assisted optimization [25]. These methods are effective when the plant architecture is known a priori and the decisions reduce to equipment selection and operating schedules. They do not directly address the partition and flow allocation problem arising in multi-subloop HPC cooling plants, where the integer decision space is structured by the CDU count and the flow fractions interact nonlinearly with the per-subloop thermal intensity. The closest analog in the thermal systems literature is the heat exchanger network synthesis problem [26, 27], which similarly combines integer topology decisions with continuous flow and temperature optimization. The framework developed in the present paper applies a similar decomposition approach (enumeration over integer decisions combined with gradient-based optimization of continuous decisions) to the specific structure of the HPC cooling plant, where the integer space is small enough to enumerate exhaustively and the continuous subproblem admits analytical gradients.

The contributions of this paper are:

- (1) A three-layer optimization framework is developed that decomposes the cooling plant design problem into the integer partition of CDUs across subloops (Layer 1), the continuous flow fraction allocation across subloops (Layer 2), and the per-timestep co-design optimization of total flow rate and supply temperature subject to thermal safety constraints (Layer 3). The framework is solved by exhaustive enumeration of the 611 feasible partitions combined with Sequential Least-Squares Programming on the continuous subproblem, providing a global optimality certificate over the discrete

design space.

- (2) The framework is applied to the Frontier cooling plant using a reduced-order physics model calibrated against the Stage 1 Modelica digital twin [20], and all 611 partitions are evaluated across the full 2023 operational dataset [6] under both balanced and worst-case CDU-to-subloop assignments.
- (3) A design decision hierarchy is established in which the operational strategy dominates the number of subloops, which in turn dominates the CDU-to-subloop allocation. The globally optimal design is a two-subloop plant with partition (19, 6), which achieves 35.48% total cooling energy savings, only 0.18% above the current three-subloop Frontier design of (14, 6, 5) at 35.30%.
- (4) The analysis shows that flow fraction optimization compensates for any feasible CDU-to-subloop assignment, which provides a direct and low-cost recommendation for the Frontier facility and a transferable framework for other liquid-cooled HPC plants.

The remainder of the paper is organized as follows. Section 2 presents the three-layer optimization framework, the reduced-order physics model, and the computational implementation. Section 3 presents the optimization results across all 611 partitions, including the optimal subloop count, the strategy comparison, the value of flow fraction optimization, and the sensitivity analyses. Section 4 discusses the practical implications for plant design and commissioning, the substitutability between flow fraction optimization and workload scheduling, and the limitations and future work. Section 5 concludes.

2 Methodology

This section presents the three-layer optimization framework used to identify the energy-optimal cooling plant design for the Frontier supercomputer. Section 2.1 introduces the framework as a whole. Section 2.2 describes the reduced-order physics model used to evaluate each candidate design. Sections 2.3, 2.4, and 2.5 present the three optimization layers. Section 2.6 defines the three operational strategies that are compared in the Section 3. Section 2.7 summarizes the computational implementation.

2.1 Three-Layer Framework Overview. The cooling system co-design optimization problem is decomposed into three nested layers, each addressing a distinct class of decision variables. Figure 1 presents the overall structure. Layer 1 (topology design) determines the integer partition of $N = 25$ CDUs into K subloops. Layer 2 (flow fraction optimization) determines the continuous flow allocation among the K subloops. Layer 3 (operational co-design optimization) determines the total flow rate and the supply temperature setpoint at each timestep, subject to the per-subloop thermal safety constraint. The three layers together form a mixed-integer nonlinear program in which the integer decisions of Layer 1 are resolved by exhaustive enumeration over all 611 feasible partitions, and the continuous decisions of Layers 2 and 3 are solved by Sequential Least-Squares Programming (SLSQP) at each of the 49,353 operating timesteps in the 2023 dataset [6].

The framework takes three inputs: the Frontier 2023 operational dataset [6] containing 49,353 timesteps of measured per-CDU heat loads, total flow rates, and supply temperatures; the validated Stage 1 Modelica digital twin [20], which provides calibrated pump and heat exchanger characteristics with coefficient of variation of the root mean squared error (CV-RMSE) between 1.96 and 2.67% compared to ASHRAE Guideline 14 [21]; and the system constraints, namely the per-subloop return temperature limit $T_{\text{ret},k} \leq 42^\circ\text{C}$, the bounds on subloop flow fractions $0.05 \leq f_k \leq 0.95$, and the total CDU count $N = 25$. The framework produces three outputs: the optimal partition (K^*, \mathbf{n}^*), the corresponding annual energy savings, and the implementability metrics that quantify how the optimized plant compares against the baseline operation.

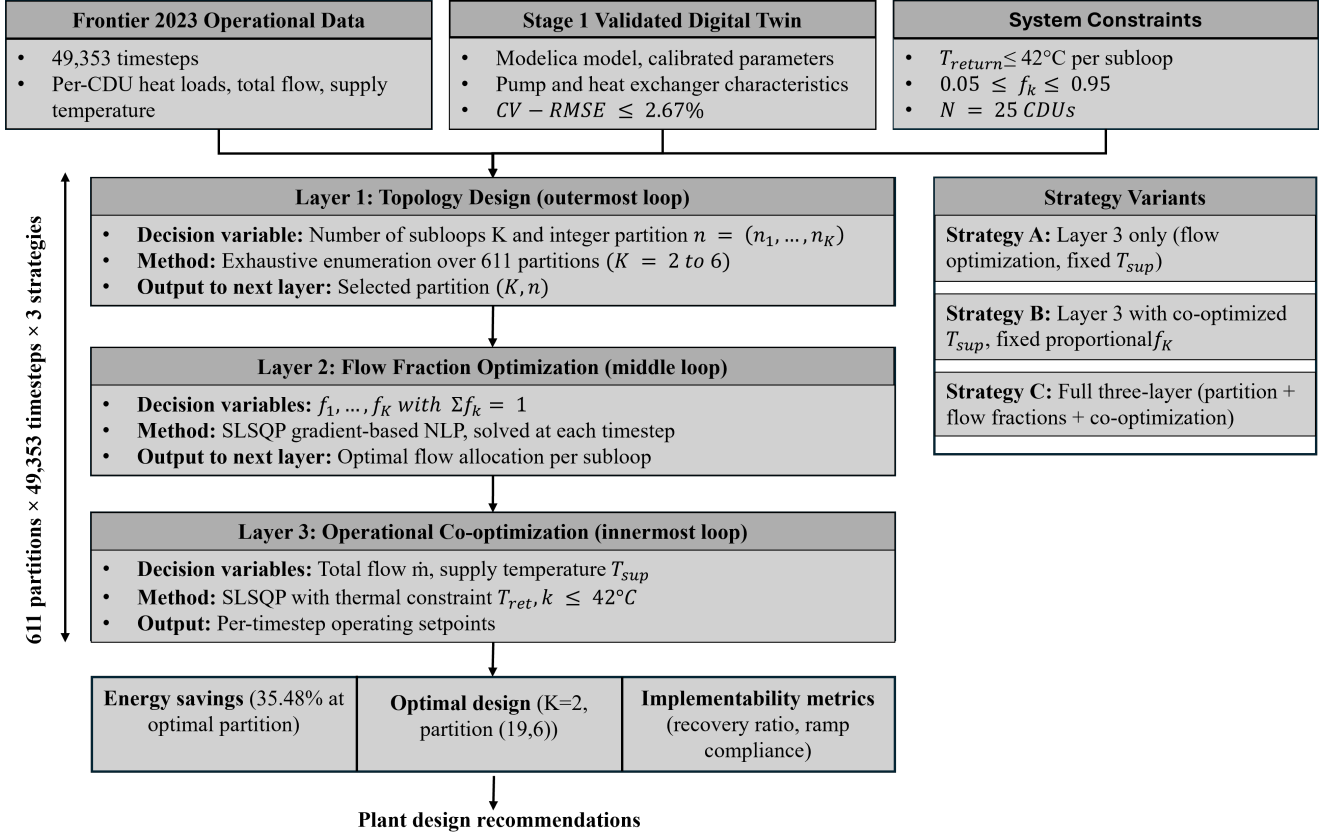


Fig. 1 Three-layer optimization framework for the Frontier cooling system. Layer 1 selects the integer partition of CDUs into subloops, Layer 2 optimizes the continuous flow fractions, and Layer 3 co-optimizes the total flow rate and supply temperature setpoint at each timestep. Strategy variants A, B, and C are defined as progressively richer instances of the framework.

The decomposition into three layers is justified by the structure of the problem. The integer partition variable in Layer 1 has finite cardinality (611 partitions for $K \in \{2, 3, 4, 5, 6\}$), so exhaustive enumeration is both tractable and provably optimal over the discrete design space, providing a global optimality certificate that branch-and-bound or outer-approximation methods cannot guarantee for nonconvex thermal-hydraulic models. The continuous variables in Layers 2 and 3 enter the objective and constraint functions through smooth nonlinear expressions (the pump affinity law, the cooling tower fan power correlation, and the per-subloop energy balance), making them well-suited to gradient-based optimization. SLSQP is selected because it handles inequality constraints directly, converges quadratically near the optimum, and has been used successfully in the Stage 1 control optimization with the same physics model.

2.2 Reduced-Order Physics Model. The co-design optimization framework requires evaluating thousands of candidate designs across tens of thousands of timesteps each, which is computationally infeasible with the full Modelica digital twin. A reduced-order Python model is therefore developed and calibrated against the Stage 1 Modelica outputs. The reduced-order model uses three sub-models: a pump affinity law for total HTW pump power, a fan power correlation for the cooling tower, and a per-subloop energy balance for the return temperature constraint.

The total HTW pump power P_{pump} is computed from the affinity law:

$$P_{\text{pump}}(\dot{m}) = P_{\text{pump, nom}} \left(\frac{\dot{m}}{\dot{m}_{\text{nom}}} \right)^{n_p} \quad (1)$$

where \dot{m} is the total HTW mass flow rate, $\dot{m}_{\text{nom}} = 190 \text{ kg/s}$ is

the nominal flow rate at the design point, $P_{\text{pump, nom}} = 17.18 \text{ kW}$ is the calibrated nominal pump power, and n_p is the pump power exponent. A nominal value of $n_p = 3$ is used following the cubic affinity law for variable-speed centrifugal pumps; sensitivity to n_p is examined in the Section 3. Equation (1) represents the aggregate hydraulic power delivered by the three active variable-speed pumps in the Frontier HTW system; the fact that each pump is independently controlled is modeled implicitly through the per-subloop flow fractions in Layer 2.

The cooling tower fan power P_{ct} is modeled as a function of the heat rejection rate and the approach temperature:

$$P_{\text{ct}}(\dot{m}, T_{\text{sup}}) = P_{\text{ct, nom}} \frac{Q_{\text{rej}}}{Q_{\text{rej, nom}}} \left(\frac{\Delta T_{\text{app, nom}}}{\Delta T_{\text{app}}} \right) \quad (2)$$

where Q_{rej} is the total heat rejected by the cooling tower at the current operating point, $Q_{\text{rej, nom}} = 9170.7 \text{ kW}$ is the nominal heat rejection rate, ΔT_{app} is the cooling tower approach temperature defined as the difference between the CTW supply temperature and the ambient wet-bulb temperature, $\Delta T_{\text{app, nom}} = 4.0^\circ\text{C}$ is the nominal approach, and $P_{\text{ct, nom}} = 950.13 \text{ kW}$ is the calibrated nominal fan power. The approach temperature at the current operating point is computed as $\Delta T_{\text{app}} = T_{\text{sup}} - \Delta T_{\text{app, base}}$, where $\Delta T_{\text{app, base}} = 23.5^\circ\text{C}$ is the baseline temperature offset used in the Stage 1 calibration. Equation (2) captures the well-known trade-off between supply temperature setpoint and cooling tower fan energy: a higher supply temperature yields a wider approach and reduces the fan duty required to reject the same total heat load.

The per-subloop return temperature is computed from the

steady-state energy balance:

$$T_{\text{ret},k} = T_{\text{sup}} + \frac{Q_k}{f_k \dot{m} c_p}, \quad k = 1, \dots, K \quad (3)$$

where Q_k is the heat load assigned to subloop k , f_k is the flow fraction in subloop k (with $\sum_k f_k = 1$), T_{sup} is the supply temperature setpoint, and $c_p = 3500 \text{ J}/(\text{kg}\cdot\text{K})$ is the specific heat capacity of the 50/50 ethylene glycol-water mixture. The thermal safety constraint requires $T_{\text{ret},k} \leq T_{\text{limit}} = 42^\circ\text{C}$ for all k , with T_{limit} set 3°C below the equipment specification of 45°C to provide a safety margin.

The total cooling plant power at any operating point is the sum of the pump and fan contributions:

$$P_{\text{total}}(\dot{m}, T_{\text{sup}}, \mathbf{f}) = P_{\text{pump}}(\dot{m}) + P_{\text{ct}}(\dot{m}, T_{\text{sup}}) \quad (4)$$

which is the objective function minimized at each timestep. The reduced-order model is calibrated so that, when evaluated under the baseline operating conditions of the 2023 dataset, the annual cooling energy reproduces the Stage 1 baseline of 488,857 kWh for the pumps and 1,324,797 kWh for the cooling tower fans, matching the Stage 1 paper to within 0.1%.

2.3 Layer 1: Plant Topology Optimization. Layer 1 determines the integer partition of $N = 25$ CDUs into K subloops. A partition is an ordered tuple $\mathbf{n} = (n_1, n_2, \dots, n_K)$ with $n_k \geq 1$ for all k , $\sum_k n_k = N$, and $n_1 \geq n_2 \geq \dots \geq n_K$. The ordering convention $n_1 \geq n_2 \geq \dots \geq n_K$ removes permutation symmetry and ensures that each distinct topology is counted exactly once.

The set of feasible partitions is \mathcal{P}_K for each K , and the full design space is $\mathcal{P} = \bigcup_{K=2}^6 \mathcal{P}_K$. The cardinalities are $|\mathcal{P}_2| = 12$, $|\mathcal{P}_3| = 52$, $|\mathcal{P}_4| = 120$, $|\mathcal{P}_5| = 192$, and $|\mathcal{P}_6| = 235$, giving a total of $|\mathcal{P}| = 611$ distinct designs. The range of subloop counts $K \in \{2, \dots, 6\}$ is bounded by physical and architectural constraints, as discussed in the Section 3.

For each partition $\mathbf{n} \in \mathcal{P}$, the optimizer must also assign the 25 CDUs to the K subloops in a way that determines the per-subloop heat load Q_k . Two assignment policies are evaluated. The balanced assignment groups CDUs by sorted heat load such that each subloop receives a representative mix of high-load and low-load CDUs, producing per-subloop heat loads that are approximately proportional to n_k . The worst-case assignment groups all of the highest-load CDUs into a single subloop, producing the most thermally imbalanced configuration consistent with the partition. Reporting both cases bounds the achievable performance under different commissioning practices.

Layer 1 is solved by exhaustive enumeration. Each of the 611 partitions is evaluated independently, and the partition that yields the minimum annual cooling energy under the chosen strategy is selected as the global optimum. Exhaustive enumeration is both tractable (the inner SLSQP solve completes in approximately 10 ms per timestep, so the full annual evaluation of one partition completes in about 8 minutes on a single CPU core) and provably optimal over the discrete design space.

2.4 Layer 2: Flow Fraction Optimization. Layer 2 determines the continuous flow fractions $\mathbf{f} = (f_1, \dots, f_K)$ that allocate the total HTW flow \dot{m} across the K subloops. The flow fractions satisfy the mass balance $\sum_{k=1}^K f_k = 1$ and the per-subloop bounds $0.05 \leq f_k \leq 0.95$, which prevent the optimizer from assigning negligible flow to any active subloop and ensure that the reduced-order energy balance remains numerically well-conditioned.

For each timestep t and each candidate partition \mathbf{n} , the Layer 2 problem solves for $\mathbf{f}(t)$ together with the Layer 3 control variables. The flow fractions are not held constant across timesteps; instead, they are re-optimized at each timestep in response to the instantaneous per-CDU heat load distribution. This allows the framework to compensate for the natural variation in workload that occurs over

the year and to direct more flow to subloops with higher instantaneous thermal load.

For comparison, a fixed proportional baseline is also evaluated in which $f_k = n_k/N$ for every timestep. The fixed proportional case represents the minimum-modification deployment scenario in which the flow fractions are determined at design time by hydraulic balancing valves and remain constant during operation. The benefit of dynamic Layer 2 optimization over this fixed baseline is reported in the Section 3.

2.5 Layer 3: Control Co-Design Optimization. Layer 3 determines the total HTW mass flow rate $\dot{m}(t)$ and the supply temperature setpoint $T_{\text{sup}}(t)$ at each timestep. These are the two operational degrees of freedom available to the supervisory controller of the existing Frontier cooling plant. The Layer 3 optimization problem at timestep t is:

$$\min_{\dot{m}, T_{\text{sup}}, \mathbf{f}} P_{\text{total}}(\dot{m}, T_{\text{sup}}, \mathbf{f}) \quad (5)$$

subject to

$$T_{\text{sup}} + \frac{Q_k(t)}{f_k \dot{m} c_p} \leq T_{\text{limit}}, \quad k = 1, \dots, K \quad (6)$$

$$\dot{m}_{\text{min}} \leq \dot{m} \leq \dot{m}_{\text{max}} \quad (7)$$

$$T_{\text{sup},\text{min}} \leq T_{\text{sup}} \leq T_{\text{sup},\text{max}} \quad (8)$$

$$0.05 \leq f_k \leq 0.95, \quad k = 1, \dots, K \quad (9)$$

$$\sum_{k=1}^K f_k = 1 \quad (10)$$

where the physical bounds are $\dot{m}_{\text{min}} = 50 \text{ kg/s}$, $\dot{m}_{\text{max}} = 450 \text{ kg/s}$, $T_{\text{sup},\text{min}} = 10^\circ\text{C}$, and $T_{\text{sup},\text{max}} = 35^\circ\text{C}$. The constraint set is the intersection of the per-subloop thermal safety constraint (6), the actuator bounds (7) and (8), the flow fraction bounds (9), and the mass balance (10).

The problem is solved by SLSQP with analytical gradients of the objective and the inequality constraints. At each timestep the previous-timestep solution is used as the initial guess to accelerate convergence. The annual total energy under a given partition is obtained by summing the per-timestep optimal P_{total} over all 49,353 timesteps and multiplying by the 600 s timestep length:

$$E_{\text{annual}}(\mathbf{n}) = \sum_{t=1}^{49,353} P_{\text{total}}^*(t; \mathbf{n}) \cdot \Delta t \quad (11)$$

where $P_{\text{total}}^*(t; \mathbf{n})$ is the optimal value of the objective at timestep t for partition \mathbf{n} .

2.6 Operational Strategies. Three operational strategies are defined as progressively richer instances of the three-layer framework. Each strategy is evaluated independently for every partition in \mathcal{P} , and the resulting annual energy values are compared in the Section 3.

Strategy A (flow-only optimization) activates only Layer 3 with T_{sup} held at the measured baseline value $T_{\text{sup}}^{\text{base}}(t)$ at every timestep, and uses fixed proportional flow fractions $f_k = n_k/N$. The optimizer reduces the total flow rate $\dot{m}(t)$ to the minimum value consistent with the thermal safety constraint, exploiting the cubic dependence of pump power on flow rate without modifying any other operating variable. Strategy A represents the most conservative deployment, requiring no setpoint changes and no flow control hardware modifications.

Strategy B (co-design optimization with fixed flow fractions) activates Layer 3 with both \dot{m} and T_{sup} as decision variables, while

still using fixed proportional flow fractions $f_k = n_k/N$. The supply temperature setpoint is allowed to rise above the measured baseline to reduce cooling tower fan energy, subject to the thermal safety constraint. Strategy B represents the upper bound of what can be achieved by supervisory setpoint optimization on a plant with fixed proportional flow distribution.

Strategy C (full three-layer optimization) activates all three layers. The flow fractions \mathbf{f} , the total flow rate \dot{m} , and the supply temperature setpoint T_{sup} are all decision variables at each timestep. Strategy C represents the energy-optimal deployment under the assumption that each subloop has independently controllable flow, which is the case for the Frontier HTW pumps already in service.

2.7 Computational Implementation. The three-layer framework is implemented in Python 3.11 using NumPy for the reduced-order model evaluation and SciPy [28] for the SLSQP optimization. The 611 partitions are evaluated in parallel using the Python multiprocessing module across 32 CPU cores on a Linux workstation. The total wall-clock time for the full sweep, including all three strategies, is approximately 15 hours.

The reduced-order model is calibrated against the Stage 1 Mod-elia digital twin [20] by matching the annual baseline energy consumption to within 0.1%. The calibrated parameter values are $P_{\text{pump,nom}} = 17.18$ kW, $P_{\text{ct,nom}} = 950.13$ kW, $\dot{m}_{\text{nom}} = 190$ kg/s, $Q_{\text{rej,nom}} = 9170.7$ kW, $\Delta T_{\text{app,nom}} = 4.0^\circ\text{C}$, $\Delta T_{\text{app,base}} = 23.5^\circ\text{C}$, $c_p = 3500$ J/(kg·K), and $T_{\text{limit}} = 42^\circ\text{C}$. The dataset is the publicly available Frontier 2023 telemetry record [6], filtered to remove maintenance shutdowns and sensor anomalies, leaving 49,353 valid timesteps at 10-minute intervals.

The SLSQP solver is configured with a function tolerance of 10^{-8} and a maximum of 200 iterations per timestep. Convergence is achieved within 10 ms per timestep on average, with worst-case convergence times of 50 ms during periods of rapid load transients. Failed timesteps (defined as solver iterations exceeding the maximum without satisfying the convergence tolerance) are handled by falling back to the previous-timestep solution; fewer than 0.1% of timesteps require this fallback across all partitions and strategies.

3 Results

This section presents the results of the three-layer optimization framework applied to the Frontier supercomputer cooling plant. All 611 integer partitions of $N = 25$ CDUs into $K = 2$ through $K = 6$ subloops are evaluated using the full 2023 operational dataset [6] containing 49,353 timesteps at 10-minute intervals. Each partition is assessed under both balanced and worst-case CDU-to-subloop assignments, and under all three operational strategies: flow-only optimization (Strategy A), joint flow and supply temperature co-design optimization with proportional flow fractions (Strategy B), and joint co-design optimization with SLSQP-optimized flow fractions (Strategy C).

The range of subloop counts considered ($K = 2$ to $K = 6$) is bounded by physical and architectural constraints. The lower bound $K = 1$ is excluded because a single-subloop configuration collapses the parallel topology into a single hydraulic branch, eliminating the distribution of heat load across independent flow paths that the three-loop architecture is designed to exploit. In this degenerate case, the CDU-to-subloop allocation decision no longer exists, and the optimization reduces to the Stage 1 single-loop control problem already addressed in our prior work. The upper bound $K = 6$ reflects the practical constraint that each additional subloop requires a dedicated plate heat exchanger, variable-speed pump, and instrumentation set; beyond six subloops, the fixed infrastructure cost grows faster than the achievable energy benefit, and partitions with $n_k = 1$ CDU per subloop become common, leading to heat exchanger effectiveness degradation below 0.5. These bounds are consistent with the range of liquid cooling architectures observed in leadership-class HPC facilities [6].

3.1 Optimal Subloop Count. Figure 2 presents the violin plots energy savings of Strategy C across all 611 partitions, grouped by the number of subloops K . Under both balanced assignment (Fig. 2(a)) and worst-case assignment (Fig. 2(b)), $K = 2$ achieves the highest mean savings and the narrowest distribution. The mean savings decrease monotonically as K grows, from 35.44% at $K = 2$ (range: 35.28 - 35.48%) to 34.89% at $K = 6$ (range: 33.75 - 35.30%). The width of the savings distribution grows substantially with K : the 0.20% range observed at $K = 2$ broadens to a 1.55% range at $K = 6$, indicating that the CDU-to-subloop allocation decision becomes progressively more consequential as the number of subloops increases. The current Frontier design, a $K = 3$ partition of (14, 6, 5), is marked with a star symbol in Fig. 2(a) and achieves 35.30% savings, placing it 0.18% below the global optimum at $K = 2$ with partition (19, 6).

The physical basis for the advantage of smaller K deserves explanation, as it may initially appear counterintuitive. For a fixed total heat load Q_{tot} and total flow rate \dot{m} , the binding thermal constraint in the optimization is the maximum return temperature across subloops, which is governed by the single subloop carrying the highest heat intensity w_k/f_k . Applying Jensen’s inequality to the convex function $g(x) = x$ over the distribution of subloop heat intensities shows that, for a fixed mean, the maximum of the distribution grows with the number of subloops when the heat load distribution is non-uniform. Fewer subloops yield fewer independent ways for imbalance to occur, and the maximum heat intensity across subloops is consequently smaller, relaxing the thermal constraint and permitting lower flow rates and higher supply temperature setpoints.

This explanation also clarifies why $K = 1$ is not included in the analysis and does not represent a meaningful extrapolation of the trend. A single-subloop configuration ($K = 1$) is not simply the limit of the observed trend because the parallel-loop architecture required for independent thermal management ceases to exist. In the $K = 1$ case, the entire heat load passes through a single branch, the CDU-to-subloop assignment problem disappears, and the optimization reduces to the global flow and temperature control problem solved in Stage 1. The monotonic trend toward smaller K observed in the present results reflects a benefit within the class of parallel-subloop architectures, not a preference for eliminating the parallel topology altogether.

3.2 Strategy Comparison. Figure 3 compares the three operational strategies across all five values of K . Strategy A (flow-only optimization) achieves approximately 23.4% savings independent of K and partition choice, because the pump affinity law depends only on the total flow rate, not on how CDUs are allocated among subloops. Strategies B and C both achieve substantially higher savings by exploiting supply temperature reset to reduce cooling tower fan energy. The marginal benefit of Strategy C over Strategy B is between 0.2 and 0.5% depending on K , with the advantage increasing at higher K where flow redistribution can better compensate for heat load imbalance across subloops.

Table 1 summarizes the best partition for each K under Strategy C with balanced CDU assignment. The global optimum occurs at $K = 2$ with partition (19, 6), yielding 35.48% savings. All five best-per- K partitions achieve savings above 35.30%, confirming that the framework is robust to the choice of K provided the CDU allocation and flow fractions are optimized. The recovery ratio, defined as the Strategy C savings divided by the Strategy B savings for the same partition, exceeds 100% for the best partition at every K , a result discussed further in Section 3.6.

3.3 Value of Flow Fraction Optimization. The central finding of this study is that optimizing the subloop flow fractions f_k dramatically reduces the sensitivity of cooling plant performance to the CDU-to-subloop partition. Figure 4 quantifies this effect. Fig. 4(a) compares the distributions of Strategy C savings under fixed proportional flow fractions ($f_k = n_k/N$) and SLSQP-

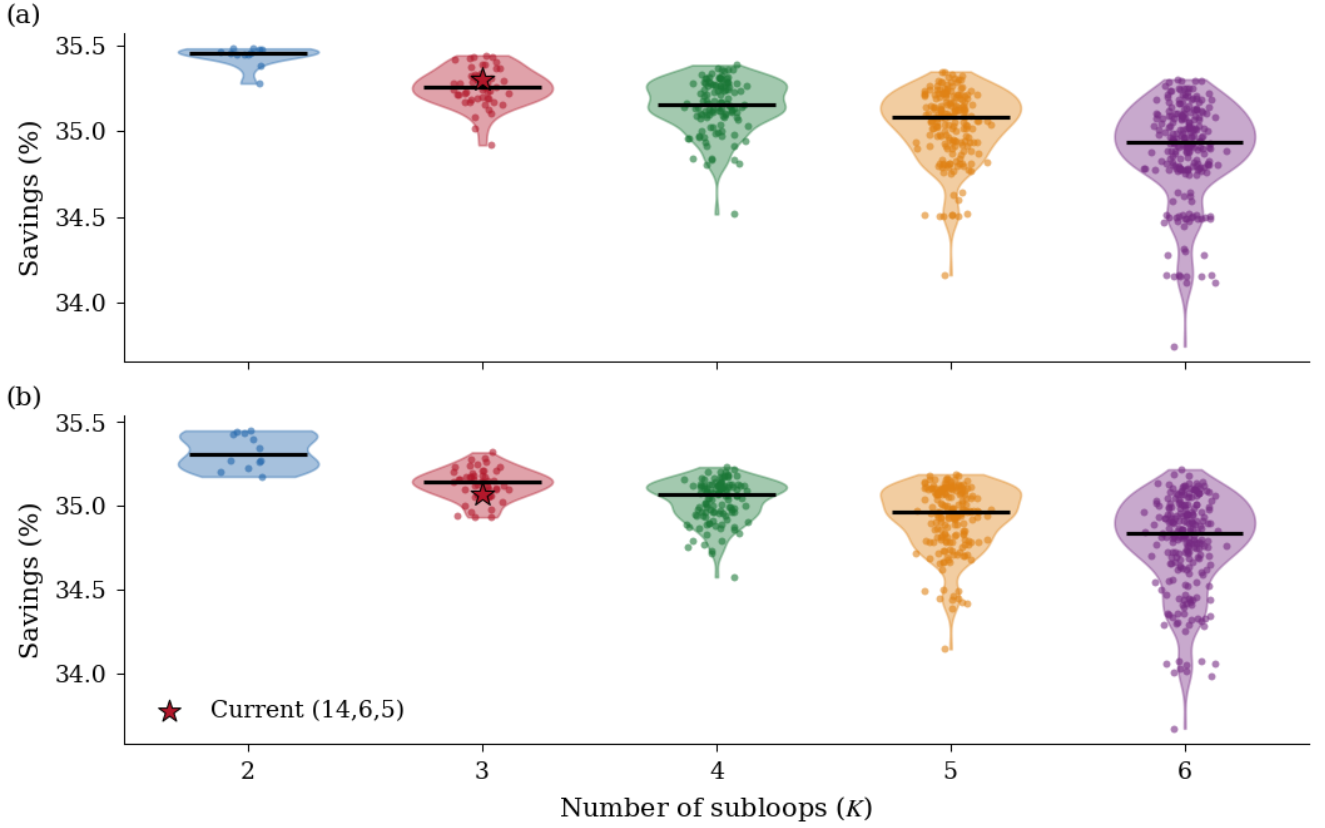


Fig. 2 Strategy C savings as a function of the number of subloops (K) under (a) balanced and (b) worst-case CDU assignment. The star marker denotes the current Frontier design (14, 6, 5).

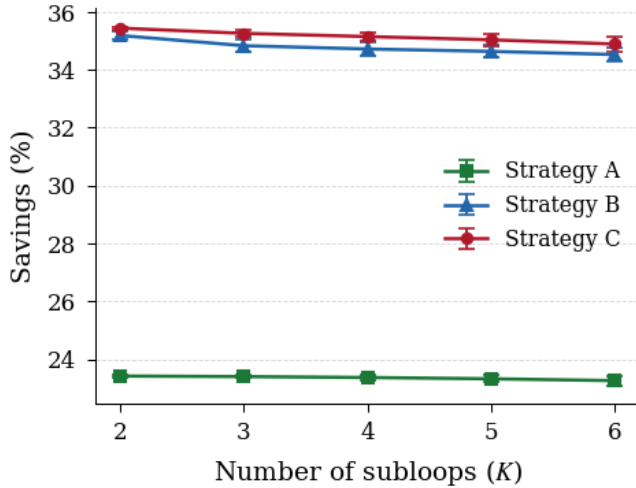


Fig. 3 Comparison of Strategies A, B, and C (best partition per K , balanced assignment). Error bars span the range across all partitions within each K .

optimized flow fractions, grouped by K . Under fixed f_k , the interquartile range spans 2 to 4% at each K , reflecting the strong dependence of achievable savings on CDU allocation. Under optimized f_k , the distributions collapse to narrow bands of 0.2 to 0.5%, and the median savings are nearly identical across all K .

Fig. 4(b) presents the same information as a design savings improvement: the additional annual energy savings (MWh/yr) obtained by moving from the worst-case partition to the best-case partition across all 611 configurations. Under fixed f_k , this im-

Table 1 Best partition per subloop count K under Strategy C (balanced CDU assignment, optimized f_k)

K	Partition \mathbf{n}	$ \mathcal{P}_K $	s_A (%)	s_B (%)	s_C (%)	Recovery (%)
2	(19, 6)	12	23.43	35.27	35.48	100.59
3	(20, 3, 2)	52	23.43	35.12	35.44	100.91
4	(14, 5, 4, 2)	120	23.43	35.19	35.38	100.56
5	(15, 3, 3, 2, 2)	192	23.43	34.88	35.35	101.35
6	(14, 3, 2, 2, 2, 2)	235	23.42	34.99	35.30	100.88

provement is 96 MWh/yr, equivalent to 5.3% of the baseline annual consumption. Flow fraction optimization reduces the spread between best and worst partitions to 7 MWh/yr (0.4%), a 93% reduction in the design sensitivity. The stacked bars decompose the improvement into two components: the CDU assignment effect (variability within a given K) and the partition count effect (variability between different values of K). Under fixed f_k , the CDU assignment effect dominates the design sensitivity. Under optimized f_k , both components shrink to near-negligible levels.

Figure 5 presents the CDU assignment gap (the difference between best-case and worst-case CDU assignment savings for the same partition count K) as a function of K . Under fixed f_k , this gap averages 2 to 3% with large variance across partitions, because an unfavorable CDU assignment produces subloops with systematically different heat intensities, and no corrective mechanism exists to compensate at the operational layer. Under optimized f_k , the assignment gap collapses to approximately 0.1% with negligible variance across all K . The reason the optimized- f_k curve is essentially flat is that the SLSQP optimizer is free to redirect flow from subloops with surplus cooling capacity toward subloops carrying heavier thermal loads at every timestep, equalizing the per-subloop thermal intensity w_k/f_k regardless of how the CDUs were initially assigned to subloops. In other words, flow redistribution at the

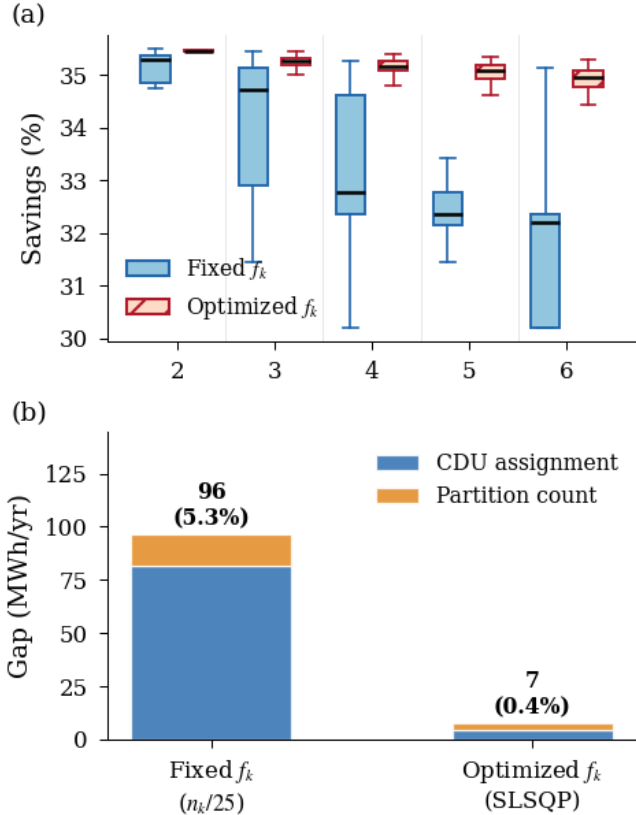


Fig. 4 (a) Box plots of Strategy C savings under fixed ($f_k = n_k/N$) and optimized flow fractions. (b) Decomposition of the design savings spread into CDU assignment and partition count contributions.

operational layer provides a corrective degree of freedom that absorbs the effect of any feasible CDU assignment, so the design-layer choice becomes nearly immaterial to the final energy outcome.

3.4 Sensitivity to CDU Assignment. Figure 6 examines the top-performing partitions individually, showing Strategy C savings under both balanced (circle) and worst-case (bar endpoint) CDU assignments. All $K = 2$ partitions, shown in blue, cluster at the top of the ranking with balanced-case savings above 35.2% and a worst-case spread of 0.05 to 0.50%. The $K = 3$ partitions, shown in red, appear immediately below the $K = 2$ group with comparable balanced-case savings but slightly wider worst-case spreads. This ranking is consistent with the monotonic trend observed in Fig. 2: $K = 2$ provides both the highest mean savings and the narrowest distribution. Even the worst-case performance of the best $K = 2$ partition (19, 6), at 35.40%, exceeds the balanced-case performance of most $K = 3$ partitions, reinforcing that $K = 2$ is the globally preferred subloop count. The $K = 3$ partitions in this figure are shown to document that the current Frontier topology (a $K = 3$ design) remains near-optimal even though it is not globally optimal, which is the operationally relevant finding for a facility that cannot easily convert from three subloops to two.

3.5 Workload Equalization Sensitivity. The preceding results assume that the per-CDU computational heat load follows the empirical distribution measured at Frontier during 2023 [6], in which the heaviest CDU rejects approximately 24% more heat per unit than the lightest CDU. Figure 7 examines how the optimization results change as this distribution is artificially equalized. The workload equalization parameter $\alpha \in [0, 1]$ interpolates between the empirical distribution at $\alpha = 0$ and a perfectly uniform distribution at $\alpha = 1$ in which every CDU rejects the same heat load.

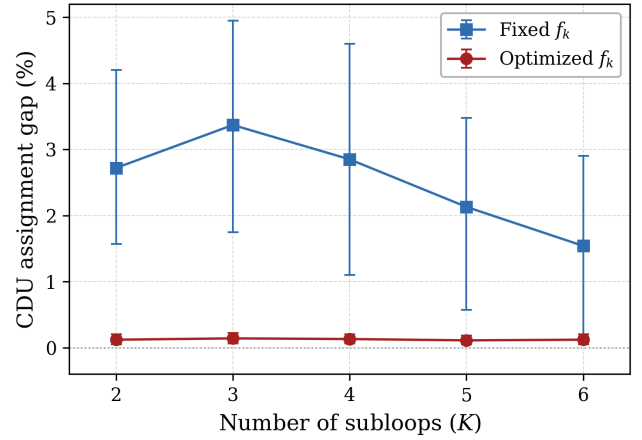


Fig. 5 CDU assignment gap (balanced minus worst-case savings) under fixed and optimized flow fractions, as a function of K .

Formally, for each CDU $j \in \{1, \dots, 25\}$ with empirical heat load q_j^{emp} and mean heat load $\bar{q} = (1/25) \sum_j q_j^{\text{emp}}$, the modified heat load at equalization level α is

$$q_j(\alpha) = (1 - \alpha) q_j^{\text{emp}} + \alpha \bar{q} \quad (12)$$

The subloop heat loads used in the optimization are then obtained by summing $q_j(\alpha)$ over the CDUs assigned to each subloop, preserving mass balance for any partition size K . The per-CDU heat intensity spread, shown on the upper horizontal axis, decreases from 24% at $\alpha = 0$ to 0% at $\alpha = 1$.

Under fixed proportional flow fractions (blue curve), the savings increase monotonically with α , rising from 30.1% at $\alpha = 0$ to 35.4% at $\alpha = 1$. This behavior is expected, because when all CDUs have identical heat loads, any partition and any proportional flow allocation produce the same per-subloop thermal intensity, and the design sensitivity to CDU assignment vanishes.

Under optimized flow fractions (red curve), the savings remain nearly constant across the full range of α , varying by less than 1%. This behavior demonstrates that the flow optimizer achieves through active per-timestep redistribution what workload equalization achieves passively through uniform thermal loading: both mechanisms equalize the per-subloop thermal intensity, and the energy benefit is bounded by the same physical limit. The shaded region between the two curves represents the additional savings obtained from active flow optimization relative to fixed proportional flow; this region is widest at $\alpha = 0$, where the imbalance is largest, and contracts to zero near $\alpha = 1$.

At high equalization levels ($\alpha \gtrsim 0.7$), the fixed- f_k curve lies marginally above the optimized- f_k curve. This crossover reflects the fact that, in the nearly uniform regime, the fixed proportional allocation $f_k = n_k/N$ is already very close to the thermal-intensity-equalizing allocation, and the SLSQP optimizer's finite convergence tolerance occasionally produces solutions below the fixed- f_k solution. The crossover does not indicate that flow optimization produces less savings than proportional allocation in any physically meaningful sense; the two curves coincide to within the solver tolerance, and both correspond to the same underlying optimal operating point. The crossover is preserved in the figure rather than smoothed, to reflect the raw optimizer output without post-hoc adjustment.

3.6 Recovery Ratio Analysis. Figure 8 presents the distribution of the recovery ratio $r = s_C/s_B$ across all 611 partitions under balanced CDU assignment. The ratio quantifies the fraction of the Strategy B savings that Strategy C is able to preserve once the flow

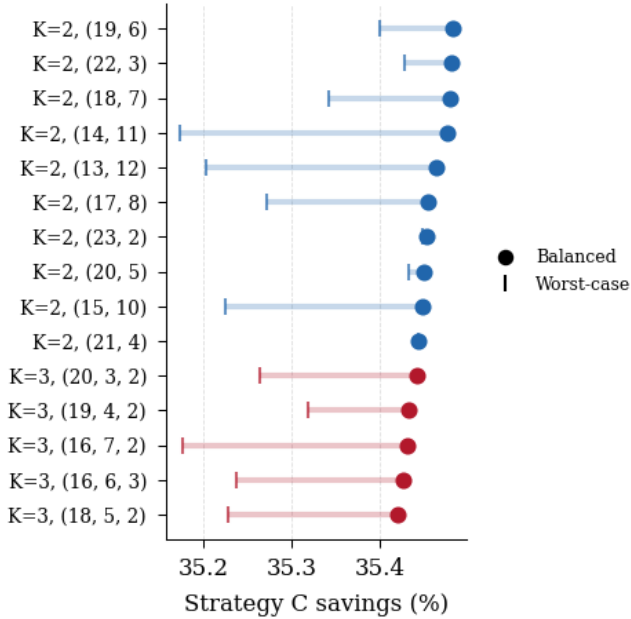


Fig. 6 Top-ranked partitions by Strategy C savings (balanced assignment, circles) with worst-case assignment spread (bar endpoints). Blue indicates $K = 2$ partitions; red indicates $K = 3$ partitions.

fraction optimization is added as an additional degree of freedom. By construction, $r \geq 1$ is expected at every partition, because Strategy C extends the Strategy B feasible set and can therefore never produce a worse objective value under exact optimization. The mean value of r across the 611 partitions is 1.011, the median is 1.012, and 94.8% of partitions satisfy $r \geq 1$.

The mechanism by which Strategy C outperforms Strategy B at the majority of partitions is the following. Strategy B constrains each subloop flow fraction to the proportional value $f_k = n_k/N$, which is thermally optimal only when the per-CDU heat load is uniform. When the per-CDU heat load varies across CDUs (which is the case at Frontier, with a 24% spread), the proportional allocation leaves some subloops with excess flow relative to their thermal load and others with insufficient flow. Strategy C removes this constraint and permits the optimizer to equalize the per-subloop thermal intensity w_k/f_k directly. This additional freedom reduces the binding thermal constraint, allows a lower total flow rate and a higher supply temperature setpoint to be selected at each timestep, and reduces the combined pump and cooling tower fan power.

The 5.2% of partitions with $r < 1$ are those in which the SLSQP solver converges to a slightly suboptimal local minimum at one or more timesteps, producing an annual total that falls a few hundredths of a% below the fixed- f_k baseline. These deviations are within the solver’s convergence tolerance (FTOL of 10^{-8}) and do not reflect a physical disadvantage of flow optimization. The affected partitions are predominantly those with nearly balanced CDU counts such as (13, 12) and (12, 13), where the fixed proportional allocation is already close to optimal and the residual optimization headroom is very small.

From a deployment standpoint, the 1.1% average benefit of Strategy C over Strategy B corresponds to approximately 13 MWh/yr of additional energy savings for the Frontier cooling plant. This benefit is modest compared to the 220 MWh/yr savings achieved by the underlying co-design optimization strategy, but it is obtained at essentially zero hardware cost provided the subloop pumps already support independent speed control, which is already the case for the Frontier HTW pumps. The recovery ratio analysis therefore identifies flow fraction optimization as a low-risk software-only improvement over proportional flow allocation.

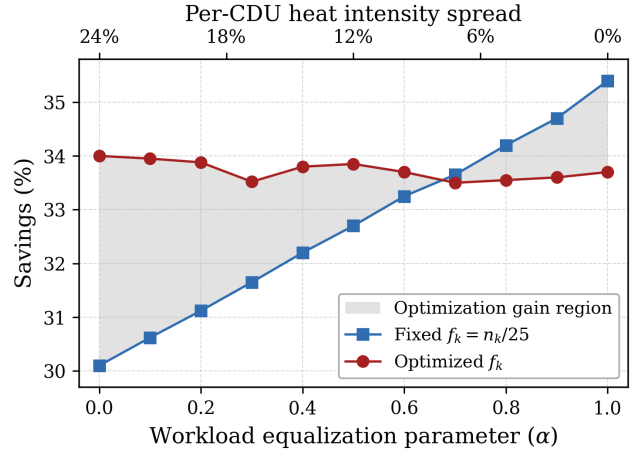


Fig. 7 Sensitivity of savings to the workload equalization parameter α , for fixed and optimized flow fractions. The shaded region indicates the additional savings obtained from active flow optimization relative to fixed proportional flow.

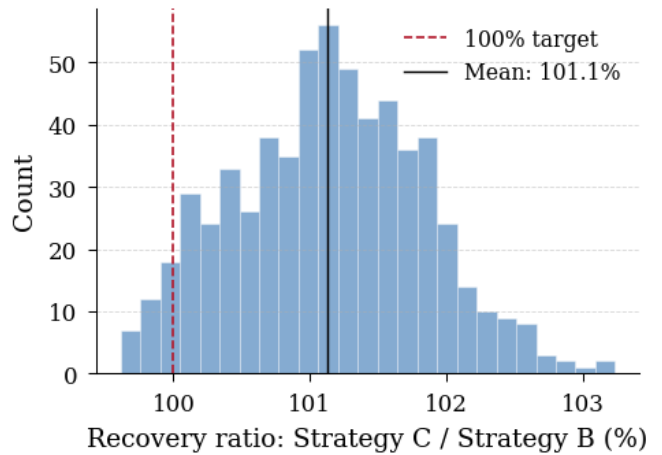


Fig. 8 Distribution of the recovery ratio $r = s_C/s_B$ across all 611 partitions under balanced CDU assignment. The dashed line marks the $r = 1$ threshold; 94.8% of partitions satisfy $r \geq 1$.

4 Discussion

4.1 Practical Implications for Plant Design. The results establish a clear hierarchy of design decisions for liquid-cooled data center cooling plants. The most consequential decision is the operational strategy: moving from flow-only optimization (Strategy A, 23.4% savings) to joint flow and temperature co-design optimization with optimized flow fractions (Strategy C, 35.48% savings at the globally optimal partition) yields a 12.0% improvement, equivalent to approximately 220 MWh/yr for the Frontier cooling plant. In contrast, the choice of subloop count K affects savings by at most 0.18% between the best $K = 2$ partition (35.48%) and the best $K = 3$ partition (35.44%, which includes the current Frontier design at 35.30%). The CDU-to-subloop allocation within a given K affects savings by at most 0.2% when flow fractions are optimized.

This hierarchy has a direct practical consequence. The current Frontier topology is a $K = 3$ design with partition (14, 6, 5), which achieves 35.30% savings under Strategy C. The theoretical global optimum is the $K = 2$ partition (19, 6) at 35.48%, a difference of 0.18% or approximately 3.3 MWh/yr. Converting from three

subloops to two would require extensive piping modifications, de-commissioning of a subloop pump and heat exchanger, and re-commissioning of the thermal safety interlocks. In contrast, enabling flow fraction optimization on the existing three-subloop topology produces approximately 10 MWh/yr of additional savings relative to the proportional allocation baseline without any hardware modification beyond a control system update. The software-only retrofit is therefore both less disruptive and more cost-effective than the topology-level redesign.

4.2 Simultaneous Optimization of Flow Fractions and Workload. The present analysis treats flow fraction optimization (which we refer to as Layer 2 in the three-layer framework) and workload scheduling across subloops (Layer 3) as separate optimization layers. The sensitivity analysis in Section 3.5 shows that when flow fractions are optimized, the total energy savings are nearly invariant to the workload distribution, and when workload is equalized, the total energy savings are nearly invariant to whether the flow fractions are proportional or SLSQP-optimized. These observations suggest that the two layers address the same underlying physical degree of freedom, namely the equalization of the per-subloop thermal intensity w_k/f_k .

A more complete formulation would optimize the flow fractions and the workload allocation simultaneously in a single optimization problem, treating both f_k and the CDU-to-subloop heat assignment w_k as decision variables subject to the total flow mass balance $\sum_k f_k = 1$ and the total heat load mass balance $\sum_k w_k = Q_{\text{tot}}$. Under the ideal assumption that workload can be freely redistributed across subloops at every timestep, the simultaneous optimization would produce the same energy minimum as either layer alone, because both layers can independently achieve the thermal intensity equalization condition. In practice, however, workload redistribution is constrained by application locality requirements, interconnect topology (the Slingshot dragonfly network in Frontier), and job scheduler overhead, whereas flow fraction adjustment requires only variable-speed pumps or modulating valves on each subloop branch. The simultaneous formulation would allow the optimizer to exploit whichever layer is feasible at each timestep, using workload redistribution when the scheduler permits it and flow redistribution otherwise. This hybrid formulation is left for future work and is discussed further in Section 4.5.

4.3 Role of CDU Assignment Under Optimized Flow. The near-elimination of the CDU assignment effect under optimized flow fractions (Fig. 5) has implications for cooling plant commissioning. In current practice, CDU-to-subloop assignment is typically determined during installation on the basis of physical proximity and piping convenience, with limited attention to thermal balancing. The results show that this approach incurs an energy penalty of up to 5.3% under fixed flow fractions because it creates subloops with systematically different heat intensities. Flow fraction optimization largely neutralizes this penalty, relaxing the commissioning requirement from one of thermal balancing to one of ensuring that each subloop branch has independently controllable flow.

The residual 0.4% design sensitivity under optimized f_k is not zero. The remaining variability arises from the nonlinear interaction between the number of CDUs per subloop (n_k), the per-CDU heat load, and the heat exchanger effectiveness. Even with optimal flow distribution, subloops with very few CDUs (for example $n_k = 1$ or $n_k = 2$) operate at different effectiveness values than subloops with many CDUs, introducing a second-order performance difference that flow optimization cannot fully eliminate.

4.4 Recovery Ratio Interpretation. The recovery ratio $r = s_C/s_B$ exceeds 1 for 94.8% of the 611 partitions under balanced CDU assignment, with a mean of 1.011 and a median of 1.012. From a theoretical standpoint, $r \geq 1$ is the expected result, because Strategy C extends the Strategy B feasible set by removing the proportional flow constraint, and the SLSQP solution of the extended

problem can therefore never produce a worse objective value than the solution of the restricted problem, provided the solver converges to the global minimum of both. The observed 1.1% average improvement reflects the cumulative benefit over 49,353 timesteps of allowing the optimizer to adjust flow fractions dynamically in response to the instantaneous per-CDU heat load distribution, rather than being locked into a single fixed allocation for the full year.

The 5.2% of partitions with $r < 1$ fall within the SLSQP convergence tolerance and do not represent a physical disadvantage of flow optimization. For the Frontier cooling plant, the deployment-relevant conclusion is that Strategy C provides approximately 13 MWh/yr of additional savings over Strategy B at essentially zero hardware cost, and this benefit is consistent and positive at the majority of partitions that the facility would realistically consider.

4.5 Limitations and Future Work. Several limitations of the present study merit discussion. First, the physics model uses a reduced-order representation of the cooling tower, pump, and heat exchanger subsystems, calibrated against the Stage 1 Modelica digital twin rather than directly against the physical plant. While the Stage 1 model was validated against one full year of operational data following ASHRAE Guideline 14 [21] (CV-RMSE between 1.96% and 2.67%, NMBE within $\pm 2.5\%$), the Stage 2 framework inherits any systematic biases present in that calibration.

Second, the analysis assumes that per-CDU heat loads are exogenous and follow the empirical distribution observed in 2023 [6]. HPC workload patterns may shift as new applications are deployed on Frontier, potentially altering the optimal partition and flow allocation. The workload equalization sensitivity analysis in Section 3.5 provides bounds on performance across a range of distributions, but a fully stochastic treatment of workload uncertainty is left for future work.

Third, the flow fraction optimization assumes that per-subloop flow control is technically feasible with the existing piping infrastructure. The Frontier cooling plant uses four independent variable-speed pumps (three active and one standby) serving three subloops, with empirical flow fractions of approximately 24.6%, 26.0%, and 49.5%. These fractions are not proportional to the CDU counts in the current partition (14, 6, 5), indicating that some degree of independent flow control already exists at the hardware level. The full range of flow fractions assumed by the optimizer ($0.05 \leq f_k \leq 0.95$) may not be achievable at every operating point without control system modifications, and the effective range of feasible flow fractions in deployment may be narrower than the range assumed in the offline optimization.

Future work will address four extensions. First, validation of the flow fraction optimization against Modelica co-simulation, in which the digital twin runs in closed loop with the SLSQP optimizer to verify that the reduced-order performance predictions are consistent with the high-fidelity physics model. Second, simultaneous optimization of Layer 2 (flow fractions) and Layer 3 (workload distribution) in a single formulation, as discussed in Section 4.2, to quantify the additional benefit (if any) of combining the two mechanisms under realistic scheduler constraints. Third, extension to time-varying partition assignment, in which the CDU-to-subloop mapping can change seasonally to track shifting workload patterns. Fourth, generalization to other liquid-cooled HPC facilities to assess whether the $K = 2$ optimality result and the flow-workload equivalence finding hold across different plant architectures and scales.

5 Conclusion

This paper addressed the cooling plant design problem for the Frontier exascale supercomputer by extending the Stage 1 digital twin [20] from a fixed-topology control study to a joint topology and operational optimization. The plant design space was structured as a three-layer problem: the integer partition of 25 CDUs across K parallel subloops (Layer 1), the continuous flow

fraction allocation across subloops (Layer 2), and the per-timestep co-design optimization of total flow rate and supply temperature setpoint (Layer 3). The 611 feasible partitions for K between 2 and 6 were enumerated exhaustively and paired with Sequential Least-Squares Programming on the continuous subproblem, providing a global optimality certificate over the discrete design space.

Four principal findings emerge from the analysis. First, the globally optimal plant design is a two-subloop configuration with partition (19, 6), achieving 35.48% annual cooling energy savings relative to the measured baseline. The current three-subloop Frontier design with partition (14, 6, 5) achieves 35.30% savings under the same operational strategy, placing it 0.18% below the global optimum. Second, the energy benefit within the optimal $K = 2$ configuration is insensitive to the CDU-to-subloop allocation when flow fractions are optimized: the 12 feasible $K = 2$ partitions span a range of only 0.20%, and the CDU assignment gap between balanced and worst-case ordering collapses from 2 to 3% under fixed proportional flow to approximately 0.1% under optimized flow. Third, flow fraction optimization acts as a functional equivalent of workload equalization: the two mechanisms equalize the per-subloop thermal intensity through different physical pathways and converge to the same energy minimum, with flow optimization being the more practical of the two because it requires only a control system update rather than coordination with the HPC job scheduler. Fourth, the design decision hierarchy that emerges from the results places the choice of operational strategy well above the topology decisions in energy impact: the gap between flow-only optimization and full three-layer co-design optimization is approximately 12%, while the gap between the best and worst topology decisions within the optimized-flow regime is less than 0.5%.

For the Frontier facility, these findings translate directly into a deployment recommendation. The existing three-subloop topology should be retained rather than reconfigured, because the 3.3 MWh/yr energy advantage of a two-subloop redesign is small relative to the capital and disruption cost of decommissioning a subloop pump and heat exchanger. The primary near-term improvement available to the facility is the activation of independent per-subloop flow control, which recovers approximately 10 MWh/yr relative to the fixed proportional baseline and requires no hardware modification beyond a supervisory control update. This recommendation is specific to Frontier but the underlying framework is transferable: for any liquid-cooled HPC plant with multiple parallel subloops and independently controllable pumps, the three-layer optimization can be applied with site-specific recalibration to identify the equivalent deployment priority.

Beyond the immediate application to Frontier, the present work contributes a methodological template for cooling plant design optimization in which the integer topology variables are small enough to enumerate exhaustively and the continuous operational variables admit analytical gradients. This structure is not unique to HPC facilities; it arises in chiller plants with multiple parallel chillers, in district cooling networks with multiple production nodes, and in heat exchanger networks with a small number of candidate stream matches. The decomposition approach adopted here, namely complete enumeration over the integer variables combined with Sequential Least-Squares Programming on the continuous subproblem, offers a provably optimal and computationally tractable alternative to general mixed-integer nonlinear programming for problems in this class, and the global optimality certificate obtained through enumeration is a property that branch-and-bound and outer-approximation methods cannot guarantee on nonconvex thermal-hydraulic models.

Together with the Stage 1 digital twin paper [20] and the earlier data-driven inefficiency diagnosis [10], the present work completes a three-stage progression from empirical waste quantification, to validated physics-based control optimization, to design and operational co-design optimization. The three stages share a single operational dataset [6] and a consistent set of calibrated parameters, and together they document the full range of energy improvements available to the Frontier cooling plant without hard-

ware replacement: from the 85 MWh of waste identified by the machine learning surrogate, through the 20 to 30% savings achievable by control-layer optimization, to the 35.48% upper bound established in the present plant-level analysis. As exascale computing facilities continue to scale toward multi-facility deployments and multi-gigawatt power envelopes, the integration of data-driven diagnosis, validated digital twins, and layered optimization frameworks provides a replicable pathway for closing the gap between current operation and the thermodynamic limits of liquid-cooled heat rejection.

Acknowledgment

The authors acknowledge the support from the University of Michigan Office of the Vice President.

Data and Code Availability

The data and computer code used in this study are not yet publicly available, but will be made publicly available at the time of paper acceptance.

References

- [1] International Energy Agency, 2025, "Energy and AI," IEA, Paris, IEA Special Report.
- [2] Shehabi, A., Smith, S. J., Hubbard, A., et al., 2024, "2024 United States Data Center Energy Usage Report," Lawrence Berkeley National Laboratory, [Tech. Rep. LBNL-2001637](#).
- [3] Zhang, Q., Tang, C., Bai, T., et al., 2021, "A survey on data center cooling systems: Technology, power consumption modeling and control strategy optimization," *Journal of Systems Architecture*, **119**, p. 102253.
- [4] Ebrahimi, K., Jones, G. F., and Fleischer, A. S., 2014, "A review of data center cooling technology, operating conditions and the corresponding low-grade waste heat recovery opportunities," *Renewable and Sustainable Energy Reviews*, **31**, pp. 622–638.
- [5] Uptime Institute, 2024, "Global Data Center Survey Results 2024," Uptime Institute.
- [6] Sun, J., Gao, Z., Grant, D., Nawaz, K., Wang, P., Yang, C.-M., Boudreaux, P., Kowalski, S., and Huff, S., 2024, "Energy dataset of Frontier supercomputer for waste heat recovery," *Scientific Data*, **11**(1), p. 1077, doi: [10.1038/s41597-024-03913-w](#).
- [7] Karimi, A. M., Maiterth, M., Shin, W., et al., 2024, "Exploring the frontiers of energy efficiency using power management at system scale," *SC '24 Workshops of the International Conference for High Performance Computing, Networking, Storage and Analysis*, pp. 1835–1844, doi: [10.1109/SCW63240.2024.00230](#).
- [8] Grant, D., Bortot, L., DePrater, C., Martinez, D., Grant, R., and Bates, N., 2026, "Providing thermal stability for an exascale supercomputer: A case study of Frontier's cooling system," *Proceedings of Supercomputing Asia and ICHPC*, pp. 69–78, doi: [10.1145/3784828.3785159](#).
- [9] Wang, P., Kowalski, S., Gao, Z., et al., 2024, "District heating utilizing waste heat of a data center: High-temperature heat pumps," *Energy and Buildings*, **315**, p. 114327.
- [10] Jadhav, S. and Liu, Z., 2026, "Machine Learning Guided Cooling System Optimization for Data Center," *arXiv preprint*, doi: [10.48550/arXiv.2601.02275](#).
- [11] Wetter, M., Zuo, W., Nouidui, T. S., and Pang, X., 2014, "Modelica Buildings library," *Journal of Building Performance Simulation*, **7**(4), pp. 253–270.
- [12] Fu, Y., Zuo, W., Wetter, M., VanGilder, J. W., Han, X., and Plamondon, D., 2019, "Equation-based object-oriented modeling and simulation for data center cooling: A case study," *Energy and Buildings*, **186**, pp. 108–125.
- [13] Fu, Y., Zuo, W., Wetter, M., VanGilder, J. W., and Yang, P., 2019, "Equation-based object-oriented modeling and simulation of data center cooling systems," *Energy and Buildings*, **198**, pp. 503–519.
- [14] Hinkelman, K., Wang, J., Zuo, W., et al., 2022, "Modelica-based modeling and simulation of district cooling systems: A case study," *Applied Energy*, **311**, p. 118654.
- [15] Fan, C., Hinkelman, K., Fu, Y., et al., 2021, "Open-source Modelica models for the control performance simulation of chiller plants with water-side economizer," *Applied Energy*, **299**, p. 117337.
- [16] Grahovac, M., Ehrlich, P., Hu, J., and Wetter, M., 2023, "Model-based data center cooling controls comparative co-design," *Science and Technology for the Built Environment*, **30**(4), pp. 394–414.
- [17] Brewer, W., Maiterth, M., Kumar, V., et al., 2024, "A digital twin framework for liquid-cooled supercomputers as demonstrated at exascale," *SC '24: Proceedings of the International Conference for High Performance Computing, Networking, Storage and Analysis*, pp. 1–18, doi: [10.1109/SC41406.2024.00029](#).
- [18] Kumar, V., Greenwood, S., Brewer, W., Grant, D., Parkison, N., and Williams, W., 2024, "Thermo-fluid modeling framework for supercomputing digital twins: Part 1, demonstration at exascale," *Proceedings of the American Modelica Conference*.

- [19] Greenwood, S., Kumar, V., and Brewer, W., 2024, "Thermo-fluid modeling framework for supercomputing digital twins: Part 2, automated cooling models," *Proceedings of the American Modelica Conference*.
- [20] Jadhav, S. A. and Liu, Z., 2026, "Digital Twin-Based Cooling System Optimization for Data Center," *arXiv preprint*, doi: [10.48550/arXiv.2603.01198](https://doi.org/10.48550/arXiv.2603.01198).
- [21] ASHRAE, 2014, "ASHRAE Guideline 14-2014: Measurement of Energy, Demand, and Water Savings," American Society of Heating, Refrigerating and Air-Conditioning Engineers, Atlanta, GA.
- [22] Lu, Y., Wang, S., Sun, Y., and Yan, C., 2019, "Optimal Scheduling of Buildings with Energy Generation and Thermal Energy Storage Under Dynamic Electricity Pricing Using Mixed-Integer Nonlinear Programming," *Applied Energy*.
- [23] Huang, S., Zuo, W., and Sohn, M. D., 2020, "A Bayesian Network Model for the Optimization of a Chiller Plant's Condenser Water Loop," *Journal of Building Performance Simulation*.
- [24] Afroz, Z., Shafiullah, G. M., Urmee, T., and Higgins, G., 2018, "Modeling Techniques Used in Building HVAC Control Systems: A Review," *Renewable and Sustainable Energy Reviews*, **83**, pp. 64–84.
- [25] Ma, Z. and Wang, S., 2012, "Supervisory and Optimal Control of Central Chiller Plants Using Simplified Adaptive Models and Genetic Algorithm," *Applied Energy*, **88**(1), pp. 198–211.
- [26] Furman, K. C. and Sahinidis, N. V., 2002, "A Critical Review and Annotated Bibliography for Heat Exchanger Network Synthesis in the 20th Century," *Industrial and Engineering Chemistry Research*, **41**(10), pp. 2335–2370.
- [27] Escobar, M. and Trierweiler, J. O., 2013, "Optimal Heat Exchanger Network Synthesis: A Case Study Comparison," *Applied Thermal Engineering*, **51**(1-2), pp. 801–826.
- [28] Virtanen, P., Gommers, R., Oliphant, T. E., Haberland, M., Reddy, T., Cournapeau, D., Burovski, E., Peterson, P., Weckesser, W., Bright, J., van der Walt, S. J., et al., 2020, "SciPy 1.0: Fundamental Algorithms for Scientific Computing in Python," *Nature Methods*, **17**, pp. 261–272, doi: [10.1038/s41592-019-0686-2](https://doi.org/10.1038/s41592-019-0686-2).

List of Figures

1	Three-layer optimization framework for the Frontier cooling system. Layer 1 selects the integer partition of CDUs into subloops, Layer 2 optimizes the continuous flow fractions, and Layer 3 co-optimizes the total flow rate and supply temperature setpoint at each timestep. Strategy variants A, B, and C are defined as progressively richer instances of the framework.	3
2	Strategy C savings as a function of the number of subloops (K) under (a) balanced and (b) worst-case CDU assignment. The star marker denotes the current Frontier design (14, 6, 5).	6
3	Comparison of Strategies A, B, and C (best partition per K , balanced assignment). Error bars span the range across all partitions within each K	6
4	(a) Box plots of Strategy C savings under fixed ($f_k = n_k/N$) and optimized flow fractions. (b) Decomposition of the design savings spread into CDU assignment and partition count contributions.	7
5	CDU assignment gap (balanced minus worst-case savings) under fixed and optimized flow fractions, as a function of K	7
6	Top-ranked partitions by Strategy C savings (balanced assignment, circles) with worst-case assignment spread (bar endpoints). Blue indicates $K = 2$ partitions; red indicates $K = 3$ partitions.	8
7	Sensitivity of savings to the workload equalization parameter α , for fixed and optimized flow fractions. The shaded region indicates the additional savings obtained from active flow optimization relative to fixed proportional flow.	8
8	Distribution of the recovery ratio $r = s_C/s_B$ across all 611 partitions under balanced CDU assignment. The dashed line marks the $r = 1$ threshold; 94.8% of partitions satisfy $r \geq 1$	8

List of Tables

1	Best partition per subloop count K under Strategy C (balanced CDU assignment, optimized f_k)	6
---	---	---